Atmospheric Environment 66 (2013) 41–51

Contents lists available at SciVerse ScienceDirect

Atmospheric Environment

journal homepage: www.elsevier.com/locate/atmosenv

Effects of soil moisture on the diurnal pattern of pesticide emission: Numerical simulation and sensitivity analysis

Rivka Reichman [a,*], Scott R. Yates [a], Todd H. Skaggs [a], Dennis E. Rolston [b]

[a] U.S. Salinity Laboratory, USDA-ARS, 450 W. Big Springs Rd., Riverside, CA 92507, United States
[b] Land, Air and Water Resources, University of California, One Shield Ave., Davis, CA 95616, United States

HIGHLIGHTS

- A framework is provided to understand temporal patterns in the volatilization rate.
- The effect of soil moisture and evaporation on the daily peak flux is elucidated.
- The model predicts different patterns for daytime or nighttime peak flux rates.
- The temporal pattern in the daily flux rate is correctly described with the model.

ARTICLE INFO

Article history:
Received 10 November 2011
Received in revised form
28 September 2012
Accepted 1 October 2012

Keywords:
Non-isothermal volatilization model
Water retention models
Soil surface resistance models
Soil temperature modeling
Pesticide vapor adsorption
Diazinon

ABSTRACT

Accurate prediction of pesticide volatilization is important for the protection of human and environmental health. Due to the complexity of the volatilization process, sophisticated predictive models are needed, especially for dry soil conditions. A mathematical model was developed to allow simulation of the diurnal variation of pesticide volatilization as affected by soil-water content, the air–solid interface partition coefficient, soil-water retention function and soil surface resistance processes. The model formulation considered two possible water retention functions and two soil surface resistance functions. To test the model, simulations were performed for ten successive days of drying under typical semi-arid summer conditions following application of the pesticide diazinon to either a loam or sand soil. Results showed that the temporal variation and magnitude of diazinon emission were strongly affected by the air–solid interface partition coefficient, soil-water content and the surface resistance function. The model was capable of simulating complex diurnal patterns in the peak emission rates which are caused by changes in soil water content and air–solid partitioning. The water retention function formulation had only a minor effect on the simulated water content and volatilization rates, whereas the soil surface resistance function significantly influenced the volatilization rate. Neither the water retention function nor the soil surface resistance formulation had a significant effect on the simulated soil temperature.

Published by Elsevier Ltd.

1. Introduction

The use of pesticides in modern agriculture has led to large increases in crop production. However, pesticide volatilization is a primary mechanism leading to the dispersion and accumulation of toxic chemicals in the environment (Taylor and Spencer, 1990; Glotfelty et al., 1984; Wang et al., 1997). Accurate prediction of volatilization rates is critical for assessing the risks of pesticide emissions to ecosystem and human health.

Volatilization rates from field soils are controlled by complex interactions between chemical properties, soil and weather conditions, and pesticide management patterns. Previous experiments have shown that diurnal variations in soil-water content and solar radiation (Glotfelty et al., 1989) or surface soil temperature (Prueger et al., 2005; Gish et al., 2009; Reichman et al., 2011) significantly affect the timing and rate of volatilization. Previous studies found that the timing of the peak volatilization rate depended primarily on the soil-water content (Glotfelty et al., 1989; Prueger et al., 2005; Gish et al., 2009; Reichman et al., 2011). When soil-water content was relatively high, the volatilization rate peaked together with solar radiation and soil temperature at mid-day. However, when soil-water content was low, the peak volatilization rate could occur at other times of day when energy inputs were lower.

* Corresponding author. Current address: Environmental Physics Department, Israel Institute for Biological Research, P.O. Box 19, Ness-Ziona 74100, Israel.
E-mail address: rikir@iibr.gov.il (S.R. Yates).

1352-2310/$ – see front matter Published by Elsevier Ltd.
http://dx.doi.org/10.1016/j.atmosenv.2012.10.002

Soil moisture status determines the partitioning of pesticide among the soil water, gas, and solid phases. Studies have shown that pesticide adsorption increases dramatically when water content falls below a critical value that signifies the point where the solid phase is no longer covered by multiple molecular layers of water (Reichman et al., 2011). For example, the equilibrium vapor density of dieldrin in soil decreased by a factor of nearly 400 when the water content fell below 2% (kg kg^{-1}) (Spencer et al., 1969), but was relatively constant in wetter soil. Therefore, modeling the short-term emission rate should include vapor adsorption at the solid–gas interface (e.g., Chen and Rolston, 2000) and an accurate estimation of soil-water dynamics near the soil surface.

Soil-water dynamics are affected by the soil water retention curve, which represents the relationship between soil water content and soil matric pressure. For dry soils, Schneider and Goss (2011) found a significant temperature dependence of the water retention curve as reflected in the adsorption enthalpy value. This result was explained by the fact that under drier conditions the interactions between water molecules and mineral surfaces are stronger than those between pure water molecules. During the last decade several non-isothermal models were developed to simulate pesticide emission rates (Baker et al., 1996; Wang et al., 1997, 1998; Reichman et al., 2000; Scholtz et al., 2002a; Yates, 2006; Bedos et al., 2009). Some of the models were tested and good order-of-magnitude agreement was found between the simulated and measured volatilization fluxes (Baker et al., 1996; Scholtz et al., 2002b; Yates, 2006; Bedos et al., 2009). However, difficulties were noticed in simulating volatilization rates under dry conditions where the timing of the daily peak flux rate was not correctly predicted.

The present paper describes a mathematical model and theoretical investigation focusing on the impact of pesticide vapor adsorption to the soil particles and soil moisture modeling on the predicted diurnal pattern of pesticide emission. The aim of this paper is to investigate the effect of different formulations proposed to improve the description of soil-water dynamics in the upper soil layer on the diurnal variation of pesticide emission. For simulation, we use a comprehensive non-isothermal volatilization model (Reichman et al., 2000), the chemical properties of diazinon (O, O diethyl O-(2-isopropyl-4-methyl-6-pyrimidinyl) phosphorothioate), soil properties for a loam or sand, and meteorological data collected near Rehovot, Israel during 1995. A companion paper (Reichman et al., 2013) will utilize the model to study pesticide volatilization under field conditions.

2. Model description

A1-D non-isothermal model was used to simulate heat, water and pesticide transport in a variably-saturated porous medium (Reichman et al., 2000). In the present study, modifications were made to account for vapor adsorption at the solid–gas interface and to examine different formulations proposed to model soil drying.

2.1. Transport equations in soil

2.1.1. Heat transport in the soil

Heat transport in the soil ($z < 0$) is expressed by the Fourier conduction equation:

$$\frac{\partial[C(\theta)T_s(z)]}{\partial t} = \frac{\partial}{\partial z}\left(\lambda(\theta)\frac{\partial T_s(z)}{\partial z}\right) \tag{1}$$

where C is soil heat capacity per unit volume (J m^{-3} °K^{-1}), T_s is soil temperature (°K), λ is soil thermal conductivity (J s^{-1} m^{-1} °K^{-1}), θ is the volumetric water content (m^3 m^{-3}) and z is soil depth (m). Both soil heat capacity and soil thermal conductivity depend on soil composition and water content, and are estimated with the method of De Vries (1963).

2.1.2. Water transport in the soil

Water transport in the soil was based on the theory of Philip and de Vries (1957), where movement is due to an isothermal part driven by the water content gradient and a thermal part driven by the temperature gradient. The transport equation for soil water (liquid and vapor) is

$$\frac{\partial\theta}{\partial t} = \frac{\partial}{\partial z}\left[D_\theta\frac{\partial\theta}{\partial z}\right] + \frac{\partial}{\partial z}\left[D_T\frac{\partial T_s}{\partial z}\right] + \frac{\partial K}{\partial z} \tag{2}$$

where K is the hydraulic conductivity (m s^{-1}), $D_\theta = D_{\theta liq} + D_{\theta vap}$ is the isothermal moisture diffusivity (m^2 s^{-1}), and $D_T = D_{Tliq} + D_{Tvap}$ is the thermal moisture diffusivity (m^2 s^{-1} °K^{-1}). The expressions for the different diffusivities are according to Philip and de Vries (1957).

The soil water vapor density, ρ_v (kg m^{-3}), is calculated from Kelvin's law:

$$\rho_v = \rho_{vs}h_s;\quad h_s = \exp\left(\frac{\Psi g}{R_w T}\right) \tag{3}$$

where Ψ is the matric potential (MPa), g is the acceleration due to gravity (m s^{-2}), R_w is the universal gas constant for water ($=4.709\times10^{-7}$ J kg^{-1} °K^{-1}), ρ_{vs} is the saturated water vapor density at a given temperature (kg m^{-3}) and h_s is the relative humidity (dimensionless).

2.1.2.1. Brooks and Corey retention model (BC). Different transport model formulations are possible depending on how the parameters Ψ and K are specified as functions of θ. The Brooks and Corey (BC) relationship is commonly used (Brooks and Corey, 1964; Mualem, 1976):

$$\Psi = \Psi_{cr}\left(\frac{\theta-\theta_r}{\theta_s-\theta_r}\right)^{-\varphi} \tag{4}$$

$$K(\theta) = K_s\left(\frac{\theta-\theta_r}{\theta_s-\theta_r}\right)^{m} \tag{5}$$

where Ψ_{cr} is the critical soil matric potential (MPa), K_s is the hydraulic conductivity of the saturated soil (m s^{-1}), θ_s is the volumetric saturated soil-water content (m^3 m^{-3}), θ_r is the residual water content (m^3 m^{-3}), and φ and m are empirical parameters.

2.1.2.2. Silva and Grifoll retention model (SG). Silva and Grifoll (2007) modeled water retention (WR) by combining three functions for different water potential ranges: (a) the BC function from saturation to Ψ_1 (−1.5 MPa), (b) the Bradley hyper-adsorptive isotherm from Ψ_1 to Ψ_2 (−162 MPa) and (c) the Brunauer–Emmett–Teller (BET) monolayer adsorption isotherm from Ψ_2 to infinite matric potential. The BET isotherm is defined as:

$$\frac{\theta}{\theta_{wm}} = \frac{B\cdot h_s}{(1-h_s)[1+(B-1)h_s]} \tag{6}$$

$$\theta_{wm} = W_m(1-n)\rho_s/\rho_w \tag{6a}$$

where W_m is the mass of water required to cover the surface as a monolayer (kg kg^{-1}) and θ_{wm} is the associated volumetric water content, ρ_s is the density of the soil solid phase (kg m^{-3}), ρ_w is the

density of the water (kg m^{-3}), n is the porosity and B is an empirical parameter; W_m and B are BET isotherm parameters.

In the Bradley's isotherm region, where multilayer adsorption dominates, the relationship is (Bradley, 1936):

$$\ln(-\Psi) = a + b\theta \tag{7}$$

where a and b are empirical parameters that can be calculated by enforcing continuity of θ at Ψ_1 and at Ψ_2.

2.1.3. Pesticide transport in the soil

Pesticide mass balance in soil is:

$$\frac{\partial C_T}{\partial t} + \frac{\partial J_s}{\partial z} + \mu C_T = 0 \tag{8}$$

where C_T is the total pesticide concentration in the soil (kg m^{-3}), J_s is the total pesticide flux in the soil (kg m^{-2} s^{-1}) and degradation is assumed to follow a first-order process, μ (s^{-1}).

The total pesticide concentration in soil is made up of the contributions of the different phases:

$$C_T = \rho_b C_s + \theta C_l + \phi C_g \tag{9}$$

where C_s is the total adsorbed concentration (kg m^{-3}), C_l is the dissolved concentration (kg m^{-3}), C_g is the concentration in the vapor phase (kg m^{-3}), ρ_b is the soil bulk density (kg m^{-3}) and ϕ is the volumetric air content (m^3 m^{-3}).

Pesticide flux in the soil (J_s) is a sum of the vapor diffusion flux and the solution diffusion–convection flux:

$$J_s = -D_l(\theta, T)\frac{\partial C_l}{\partial z} + v_l C_l - D_g(\phi, T)\frac{\partial C_g}{\partial z} \tag{10}$$

where v_l is the average pore-water velocity (m s^{-1}), z is the vertical coordinate (increasing upward), D_l and D_g are diffusion coefficients for the chemical in soil solution and air voids (m^2 s^{-1}), respectively. In our simulations, liquid flow velocity is very small and dispersion is negligible. The effect of soil porosity and tortuosity on the diffusion coefficient in soil solution is expressed by the Millington and Quirk (1961) model and in soil air voids by the Moldrup et al. (2000) model. The dependence of the diffusion coefficients on temperature is according to Bird et al. (1960).

Partitioning of the pesticide among the three soil phases depends on both temperature and moisture content. Henry's law describes the partitioning between soil liquid and vapor phases, where the dimensionless Henry constant, K_H, is temperature-dependent.

The total adsorbed concentration, C_s (kg m^{-3}), is the sum of chemical adsorbed at the solid–liquid interface, C_{sl}, and the solid–air interface, C_{sg} (Chen and Rolston, 2000),

$$C_s = C_{sl} + C_{sg} \tag{11}$$

where

$$C_{sl} = [1 - \alpha_g(\theta_g)]K_d C_l; \quad C_{sg} = \alpha_g(\theta_g)K_g C_g$$

and

$$\alpha_g(\theta_g) = \frac{S_0}{SSA} = \frac{1 - x(\theta_g)}{1 - x(\theta_g) + Bx(\theta_g)} \tag{12}$$

where $[1 - \alpha_g(\theta_g)]$ is the fraction of soil surface area covered by water molecules, S_0 is the surface area not covered by water molecules (m^2 kg^{-1}), SSA is the specific surface area (m^2 kg^{-1}), B is the BET isotherm parameter, θ_g is gravimetric water content (kg kg^{-1}), K_d and K_g are, respectively, the partitioning coefficients at the solid–water and solid–air interfaces (m^3 kg^{-1}) and x is calculated using the empirical expression

$$x(\theta_g) = \exp[-\xi\exp(-\zeta\theta_g)] \tag{13}$$

where ξ and ζ are fitting parameters. Chen et al. (2000) give a detailed description of methods for determining the various empirical coefficients. The partition at the solid–water interface is assumed to be controlled by the soil organic matter.

2.2. Heat and vapor transfer through the atmospheric boundary layer

The surface boundary fluxes are calculated assuming the existence of a constant flux layer that extends to a few meters above the surface roughness height, z_0 (m). The atmospheric surface layer fluxes for momentum, M (kg m^{-1} s^{-2}), and heat, H (J m^{-2} s^{-1}), are given by (Reichman et al., 2000):

$$\frac{M}{\rho_a} = K_m\frac{\partial u}{\partial z} = u^{*2} \tag{14}$$

$$\frac{H}{\rho_a c_p} = K_{ah}\frac{\partial T}{\partial z} = u^* T^* \tag{15}$$

where, k (=0.4) is the von Karman constant, c_p is the air specific heat capacity (J kg^{-1} °K^{-1}) and ρ_a is the air density (kg m^{-3}). The parameters $u^*$and T^* are the surface friction velocity (m s^{-1}) and the friction potential temperature (°K), respectively, and are assumed to be constants. The parameters K_m and K_{ah} are the bulk transfer coefficients through the atmospheric surface layer for momentum and heat (m s^{-1}), respectively, and are given by:

$$K_m = \frac{ku^* z_{ref}}{\Phi_m}; \quad K_{ah} = \frac{ku^* z_{ref}}{\Phi_H} \tag{16}$$

where, Φ_m and Φ_H are dimensionless empirical functions for wind and temperature profiles that depend on atmospheric stability. The elevation z_{ref} is the height where wind velocity and air temperature were measured (usually ~2 m).

Using expressions for Φ_m and Φ_H (see Businger, 1973) in Eq. (16) and using Eqs. (14) and (15), H can be written as

$$\frac{H}{\rho_a c_p} = \frac{ku^*}{0.74[\ln(z/z_0) - \psi_2]}(T_a - T_0) \tag{17}$$

where T_a is the air temperature measured at z_{ref}, T_0 is the surface temperature (°K), and ψ_1 and ψ_2 are dimensionless empirical atmospheric stability functions. H can also be written in terms of atmospheric resistance, r_a, as,

$$\frac{H}{\rho_a c_p} = \frac{1}{r_a}(T_a - T_0) \tag{18}$$

It is commonly assumed that heat, humidity and trace gases have the same bulk transfer coefficients through the atmospheric surface layer (i.e., $1/r_a$), therefore the latent heat flux, E_w (kg m^{-2} s^{-1}), and pesticide flux, F (kg m^{-2} s^{-1}), are:

$$\frac{E_w}{\rho_a L} = \frac{1}{r_a}[q_a - q(z_0)] \tag{19}$$

$$F = \frac{1}{r_a}[C_a - C(z_0)] \tag{20}$$

where q_a and q (z_0) are the absolute humidity in air (kg m^{-3}) measured at z_{ref} and z_0, respectively, L is the latent heat of evaporation (=2.45 × 10^6 J kg^{-1}), and C_a and C (z_0) are the pesticide concentration in air (kg m^{-3}) measured at z_{ref} and z_0, respectively.

The pesticide concentration at the soil roughness height, C (z_0), is assumed to be equal to the pesticide concentration at the soil surface, C $(z = 0)$.

2.2.1. The energy balance equation

The temperature at the soil surface, T_0, was determined by the energy balance equation:

$$R_n = H + E_w + S \tag{21}$$

where R_n, H, E_w and S are the net radiation, sensible, latent and soil heat fluxes (J m^{-2} s^{-1}), respectively. The net radiation is given by

$$R_n = (1 - \alpha)R_g + \varepsilon R_L - \varepsilon\sigma T_0^4 \tag{22}$$

where R_g is the global radiation (J m^{-2} s^{-1}), R_L is the atmospheric long wave radiation (J m^{-2} s^{-1}), α is the soil albedo, ε is the soil emissivity, and σ is the Stefan–Boltzmann constant (=5.69 × 10^{-8} J m^{-2} s^{-1} °K^{-4}). The soil heat flux is

$$S = \lambda \left.\frac{\partial T_s}{\partial z}\right|_{z=0} \tag{23}$$

2.2.2. Soil surface resistance (SSR) and wetness function

2.2.2.1. van de Grind and Owe soil surface resistance model (VDG). Beginning with wet topsoil, evaporation commences at the soil surface. As the topsoil dries, the phase change occurs at some depth below the surface with a transition zone from the surface to the evaporation front. The transport of water is due to vapor diffusion. The dry surface layer acts as a barrier to vapor transport, so the total resistance can be modeled as the sum of the atmospheric and soil resistance ($r_a + r_s$) terms (Bittelli et al., 2008; van de Griend and Owe, 1994),

$$\frac{E_w}{\rho_a L} = \frac{1}{r_s + r_a}[q_a - q(z_0)] \tag{24}$$

The soil resistance term is defined as (van de Griend and Owe, 1994),

$$r_s = 10\exp[0.3563(\theta_{min} - \theta_{top})] \tag{25}$$

where θ_{min} (%) is an empirical minimum above which the soil is able to deliver vapor at a potential rate, and θ_{top} (%) is the volumetric soil-water content of the top 0.01 m layer. The factor 10 was obtained from studies of molecular diffusion of water surfaces (La Mer and Healy, 1965).

2.2.2.2. Deardorff soil surface resistance model (D). The absolute humidity at z_0 is often given by $q(z_0) = q_{sat}(T_0)\cdot h_s$, where, $q_{sat}(T_s)$ is the saturated value of absolute humidity (kg m^{-3}) at soil surface temperature, T_0 (°K). An alternative approach to estimate absolute humidity that is often used in atmospheric circulation models (Lee and Pielke, 1992) is

$$q(z_0) = \beta q_{sat}(T_0) + (1 - \beta)q_a \tag{26}$$

where β is a wetness function. Substituting Eq. (26) into Eq. (24), the following expression for the evaporation rate is obtained:

$$\frac{E_w}{\rho_a L} = \frac{1}{r_s + r_a}\beta[q_{sat}(T_0) - q_a] \tag{27}$$

where β can be obtained using Deardorff's formula (Deardorff, 1978):

$$\beta = \min\left(1, \frac{\theta}{\theta_{fc}}\right) \tag{28}$$

where θ_{fc} is the soil-water content at field capacity (m^3 m^{-3}).

2.3. Boundary and initial conditions and numerical solution

At the soil–atmosphere interface, $z = 0$, we assume equivalence in the soil and atmospheric fluxes for water and chemical.

$$J_w|_{z=0} = E_w|_{z=0}; \quad J_s|_{z=0} = F|_{z=0} \tag{29}$$

where J_w is the water flux in the soil, E_w is the latent heat flux in the atmosphere determined by either (19), (24) or (27), J_s is the chemical flux in the soil, and F is the pesticide volatilization flux in the atmosphere determined by (20).

At the lower boundary of the soil profile, a constant temperature and zero water and chemical fluxes were assumed,

$$J_w = J_s = 0 \quad \text{at} \quad z = L_c \tag{30}$$

The initial soil temperature and moisture are uniformly distributed with depth. Their values depend on the seasonal weather conditions. The initial pesticide distribution in the soil profile is

$$\begin{aligned} C_T(z,0) &= C_0 \quad \text{if} \quad 0 > z > -L_i \\ C_T(z,0) &= 0 \quad \text{if} \quad z < -L_i \end{aligned} \tag{31}$$

where L_i is the depth of the soil layer in which the chemical is initially incorporated.

The nonlinear partial differential equations and boundary conditions were solved numerically using finite differences. The diffusion terms were approximated by a modified Crank–Nicholson scheme (Avissar and Mahrer, 1982) and the convection terms by a space-centered scheme. The mass and temperature balance equations were solved simultaneously by the Newton–Raphson iteration procedure. Grid discretization of 0.1, 0.5, 1.0, 5.0, and 10.0 mm were used for soil layers 0–1.0, 1.0–1.5, 1.5–3.0, 3.0–5.0, and 5.0–20.0 cm, respectively. The temporal discretization was forward in time. The time step of the integration was 10 min based on a preliminary study that confirmed10 min was adequate to achieve convergence.

3. Numerical simulations

Numerical simulations were performed to determine the sensitivity of diurnal patterns of pesticide volatilization with respect to: (1) the soil air–solid interface partition coefficient (K_g) and soil-water content; and (2) the WR and SSR functions. The effect of the different possible water retention (WR) and soil surface resistance (SSR) formulations on the simulated soil-water content and soil temperature were also examined. For WR, the full-range function of Silva and Grifoll (2007) (SG) and the Brooks and Corey (BC) function were evaluated. Two SSR methods were also

evaluated: the Deardorff, 1978 approach (D) and the van de Griend and Owe, 1994 approach (VDG), which leads to the following (WR × SSR) combinations: BC-D, BC-VDG, SG-D and SG-VDG.

Numerical simulations were performed for typical semi-arid summer conditions following a hypothetical application of diazinon (Table 1) to two soils: loam and sand (Table 2). The BC and SG WR models for the two soils are presented in Fig. 1. By definition, the two WR functions deviate only below the wilting point ($\Psi_1 = -1.5$ MPa). For both soils, the suction values calculated using the SG WR model were lower than those calculated using the BC WR model for all water contents below the wilting point. Diazinon is a relatively non-polar pesticide in which adsorption to soil particles is significantly affected by soil-water content (Spencer et al., 1982; Chen et al., 2000).

The variations of the input meteorological parameters are shown in Fig. 2. These parameters represent a typical day in August 1995 in Rehovot. The maximum solar radiation was about 1000–1100 W m^{-2} (Fig. 2a). The air temperature, relative humidity and wind speed, respectively, varied between 21 and 31 °C, 44 and 95 % and 0.4 and 4.8 m s^{-1} (Fig. 2b–d).

The simulated soil temperature and water content for the loam soil at 0.01 and 0.05 m are presented in Figs. 3 and 4, respectively. The initial water content was 0.2, a value in the range where liquid water flow dominates, and between the field capacity (0.27) and the wilting point (0.12). After 10 days of drying using the BC-D model, the soil-water content at 0.01 and 0.05 m, respectively, dropped to about 0.06 and 0.087 (Fig. 4). The soil temperature varied between 22 and 43 °C depending on soil depth and local moisture condition, with larger diurnal variations observed at 0.01 m and for dryer soil conditions (Fig. 3).

For the Rehovot sand simulations, the initial water content was 0.08 (field capacity was 0.09; wilting point was 0.03), and the overall behavior was similar to the loam simulations. The predicted soil-water content fell to about 0.027 and 0.036 for the depths of 0.01 and 0.05 m, respectively (Fig. 5) and the soil temperature varied between 22 and 46 °C depending on soil depth and local moisture levels (data not presented).

Table 1
Diazinon properties used for simulation.

Property	Value
Molecular weight	0.304 kg mol^{-1}
Water solubility	2.22 g mol^{-1}
Air diffusion coefficient[a]	4.83 × 10^{-6} m^2 s^{-1}
Water diffusion coefficient[b]	4.17 × 10^{-10} m^2 s^{-1}
Degradation coefficient[c]	0.03 d^{-1}
Sorption coefficient	
Soil water-organic matter partitioning coefficient (K_{om})[d]	1.52 m^3 kg^{-1} OM
Soil air–solid interface partitioning coefficient (K_g)[e]	1.1 × 10^7 m^3 kg^{-1}
Fitting parameters for $x(\theta_g)$ Eq. (13)[f]	
ξ	12.1 (loam and sand)
ζ	60.28 (loam), 544 (sand)
Vapor pressure-temperature relation[g]	P (Pa) = $0.0075 \cdot 10^{9.3871 - 4014.67/T\,(^\circ K)}$

[a] The diazinon diffusion coefficient in air was calculated using the Fuller et al. (1966) expression.
[b] The diazinon diffusion coefficient in water was taken from Lin et al. (1996).
[c] Loam soil (20–30 °C). From Bro-Rasmussen et al. (1970).
[d] Based on $K_d = 0.023$ m^3 kg^{-1} measured for Yolo silt loam soil that contains 1.5% organic matter (Chen et al., 2000).
[e] Based on measurement of diazinon vapor adsorption to Yolo silt loam (Chen et al., 2000).
[f] The parameters were fitted to measurements taken for red brown loam from North Auckland (Orchiston, 1952) and sand (Ruiz et al., 1998).
[g] The temperature-dependent vapor pressure relationship (Kim et al., 1984) was measured using the gas saturation method.

Table 2
Soil properties used for simulation.

Property	Loam soil[a]	Rehovot sand[b]
Soil physical properties:		
Sand/silt/clay	40/40/20 (%)	99/1/0 (%)
Organic matter	1%	0.1%
Bulk density	1500 kg m^{-3}	1200 kg m^{-3}
Porosity	0.463 m^3 m^{-3}	0.40 m^3 m^{-3}
Hydraulic properties:		
K_{hs}	3.7 × 10^{-6} m s^{-1}	7.64 × 10^{-5} m s^{-1}
m	5.5	3.2
φ	4	1.2
ψ_{cr}	−0.40 m	−0.25 m
θ_s	0.434 m^3 m^{-3}	0.4 m^3 m^{-3}
θ_r	0.027 m^3 m^{-3}	0.015 m^3 m^{-3}
θ_{fc} (Ψ = −33 kPa)	0.27 m^3 m^{-3}	0.09 m^3 m^{-3}
θ_1 (Ψ = −1.5 MPa)[c]	0.12 m^3 m^{-3}	0.03 m^3 m^{-3}
θ_{min}[d]	15%	15%
Water adsorption isotherm:		
BET isotherm parameters[e]:		
B	15.2	7.11
W_m	0.033 kg kg^{-1}	5.24 × 10^{-4} kg kg^{-1}
Bradley isotherm parameters[f]:		
a	16.47	14.54
b	−83.16	−324.71
Photometric properties[g]:		
Short wave radiation:		
Albedo	0.2	0.25
Absorption	0.8	0.75
Long wave radiation:		
Reflectivity	0.1	0.1
Absorption	0.9	0.9
Emissivity	0.9	0.9

[a] Soil texture properties were according to the mid-value of USDA classification. The hydraulic properties and soil porosity were according to the Arithmetic average for loam soil (Rawls et al., 1982).
[b] Soil texture and hydraulic properties according to soil #4121 in Mualem (1976).
[c] This value corresponds to the wilting point.
[d] This parameter was estimated using Eq. (25) and measured surface resistance for fine sandy loam with fast air circulation chamber (van de Griend and Owe, 1994).
[e] Loam soil and Rehovot sand parameters were according to red brown loam from North Auckland (Orchiston, 1952) and sand (Ruiz et al., 1998), respectively.
[f] Estimated according to the procedure suggested in Silva and Grifoll (2007).
[g] Avissar and Mahrer (1988).

3.1. Sensitivity to K_g

The sensitivity of the pesticide flux to K_g was performed using BC-D model formulation. The values of K_g were 1.1 × 10^7 (Chen et al., 2000), 1.1 × 10^6, 1.1 × 10^5, 1.1 × 10^4, 1.1 × 10^3 and 0 m^3 kg^{-1}. The effect of K_g on diazinon volatilization for the loam and sand soils, respectively, are summarized in Figs. 6 and 7. Fig. 7 shows only the first four days because no significant change in the diurnal pattern was observed afterwards. The maximum and minimum volatilization rates obtained over time for both soils with the different values of K_g are presented in Fig. 8.

In both soils, the timings of the diurnal peak flux for $K_g = 0$ were different from simulations with high K_g values. With $K_g = 0$ (i.e., no vapor adsorption), high flux rates occurred mid-day (13:00) and low fluxes occurred at night (5:00), which followed the behavior of the solar radiation (Fig. 2) and soil temperature (Fig. 3). For high K_g values ($\geq$1.1 × 10^5 m^3 kg^{-1}), the flux rates had an inverse relationship, with morning peak values (8:00) and afternoon minima (15:00) (Figs. 6 and 7). For nonzero K_g, drying of the surface layer significantly reduced the maximum and minimum flux rates over time (Fig. 8).

In other respects, the two soils exhibited different sensitivities to K_g. For midrange K_g values, the shape of the flux rate curves for the loam soil initially followed $K_g = 0$, but transitioned to the shape observed for high K_g. For instance, with K_g = 1.1 × 10^4 m^3 kg^{-1} in the loam soil, the high K_g pattern was observed after approximately

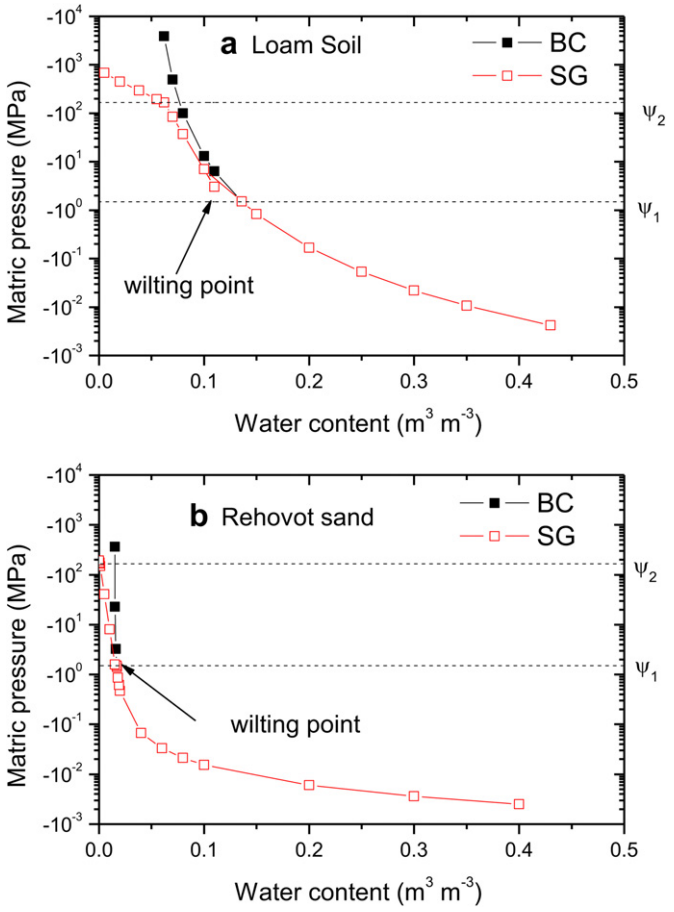

Fig. 1. Water retention curves for BC and SG WR models for (a) loam soil and (b) Rehovot sand. $\Psi_1 = -1.5$ MPa and $\Psi_2 = -162$ MPa.

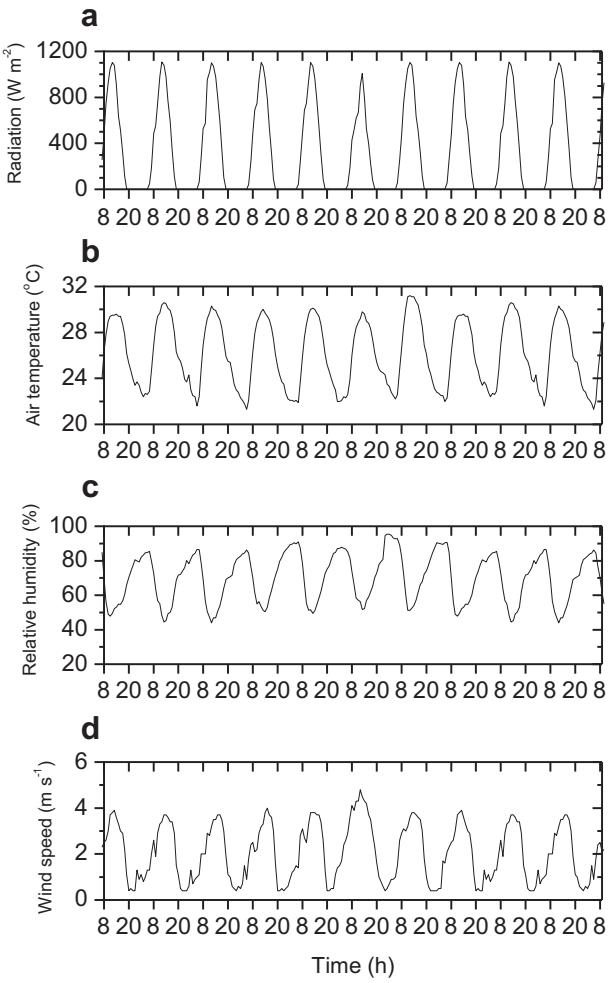

Fig. 2. The diurnal variation of the meteorological parameters used as input for simulation.

3 days (Fig. 6). In the sand, when $K_g \leq 1.1 \times 10^4$ m^3 kg^{-1} the shape of the flux curve was similar to the $K_g = 0$ curve throughout the simulation (Fig. 7), and significantly less reduction in the volatilization peaks values was observed (Fig. 8), which indicates there was limited vapor adsorption to sand with $K_g \leq 1.1 \times 10^4$ m^3 kg^{-1}. The progression from a diurnal flux rate pattern that follows the solar radiation and soil temperature to a pattern with an inverse relationship is most noticeable for $0 \leq K_g \leq 1.1 \times 10^4$ m^3 kg^{-1} and loam soil (Fig. 6). For $K_g = 1.1 \times 10^3$ m^3 kg^{-1}, the flux rate during the first day was similar to the $K_g = 0$ curve while the soil-water content at 1 cm was 0.2–0.12. Afterwards, as the soil dried, the timing of the mid-day peak was earlier and its magnitude was relatively lower. The timing of the minimum flux rate remained nearly the same.

These results agree with field measurements where, as soil dried, the peak emission occurred during the morning instead of mid-day hours and the flux rate was lower (Glotfelty et al., 1989; Bedos et al., 2009; Pattey et al., 1995; Prueger et al., 2005; Gish et al., 2009; Reichman et al., 2011). This phenomenon has been attributed to the effect of soil-water on pesticide adsorption to soil particles. In wet soils, water displaces the chemical from the surface of the soil particles which leads to increased vapor pressure (Spencer and Cliath, 1970, 1973). As the water content decreases below a threshold level, the vapor pressure rapidly decreases to near zero values. This process reverses upon wetting. Therefore, increases in water content due to condensation or upward transport would decrease vapor sorption and increase the pesticide flux rate.

Fig. 9a and b shows the cumulative flux after 10 days of drying for loam and sand, respectively. A negative linear relationship

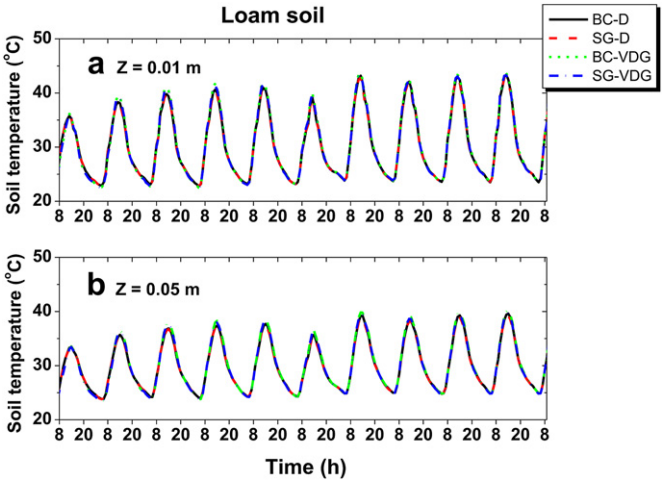

Fig. 3. The effect of the tested models on simulated soil temperature in the loam soil at (a) 1 cm and (b) 5 cm (BC = Brooks–Corey water retention function; SG = Silva and Grifoll (2007) full-range water retention model; D = the β wetness surface resistance function of Deardorff (1978); VDG = the surface resistance function proposed by van de Griend and Owe (1994)).

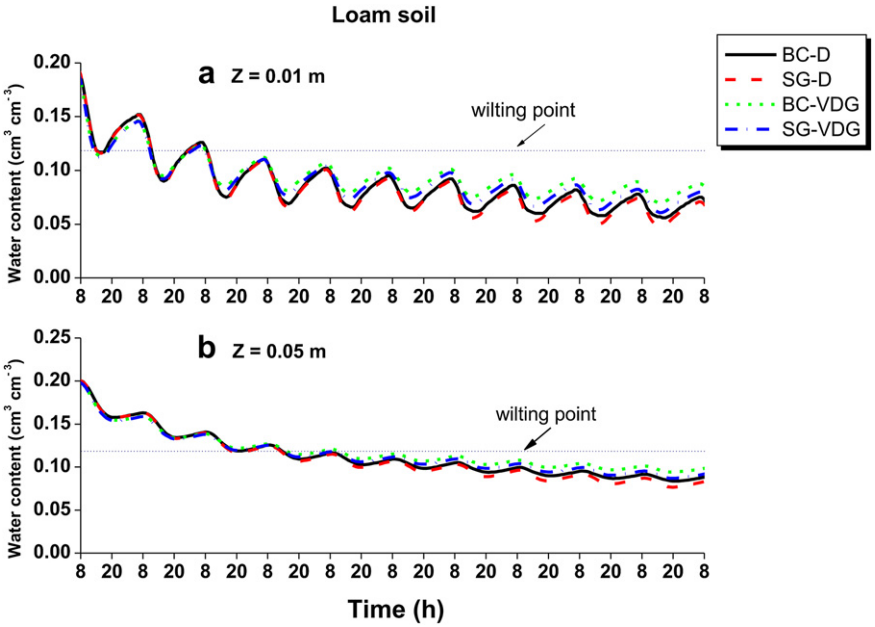

Fig. 4. The effect of the tested models on simulated water content in the loam soil at (a) 0.01 m and (b) 0.05 m (BC = Brooks–Corey water retention function; SG = Silva and Grifoll (2007) full-range water retention model; D = the β wetness surface resistance function of Deardorff (1978); VDG = the surface resistance function proposed by van de Griend and Owe (1994)).

between the cumulative flux and $Log_{10}K_g$ was observed over the entire range of K_g values for the loam soil (Fig. 9a), and when $K_g \geq 1.1 \times 10^4$ m^3 kg^{-1} for the sand (Fig. 9b). This behavior is consistent since vapor adsorption to sand is limited for $K_g \leq 1.1 \times 10^4$ m^3 kg^{-1}. In both cases the correlation coefficient (R^2) for the linear regression was good (0.96 loam; 0.98 sand).

For high K_g ($\geq 1.1 \times 10^5$ m^3 kg^{-1}), reducing the value of K_g by an order of magnitude increased the value of the flux (maximum peak value) by a factor of 4 for the loam soil (Figs. 6 and 8). In the sand, a similar reduction increased the flux by an order of magnitude during the low flux period, but had only a minor effect on the flux during the high flux period (18:00–9:00, Fig. 7).

3.2. Sensitivity to the WR and SSR functions

Sensitivity tests were conducted for the four (WR × SSR) model formulations. Since $K_g = 1.1 \times 10^5$ m^3 kg^{-1} was found to be

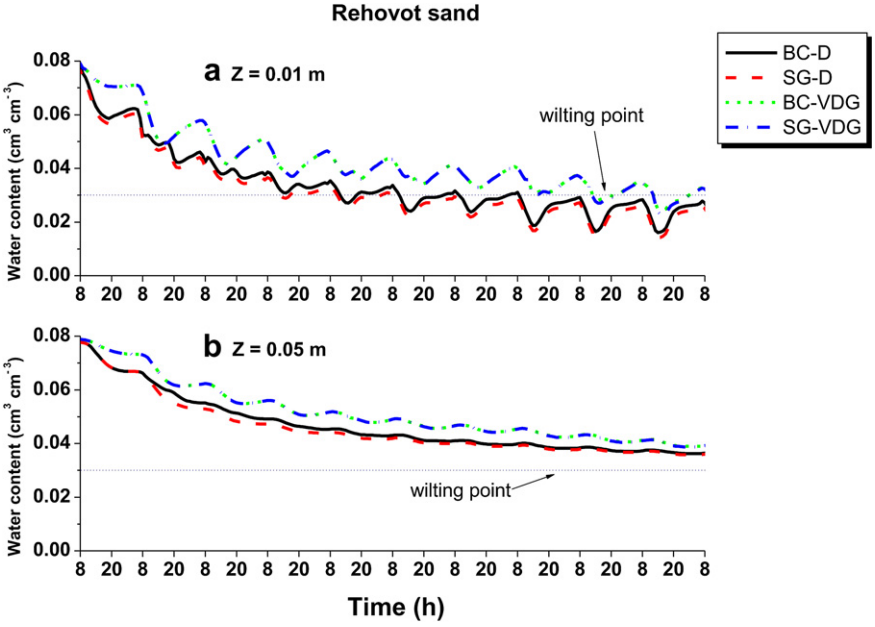

Fig. 5. The effect of the tested models on simulated water content in Rehovot sand at (a) 0.01 m and (b) 0.05 m (BC = Brooks–Corey water retention function; SG = Silva and Grifoll (2007) full-range water retention model; D = the β wetness surface resistance function of Deardorff (1978); VDG = the surface resistance function proposed by van de Griend and Owe (1994)).

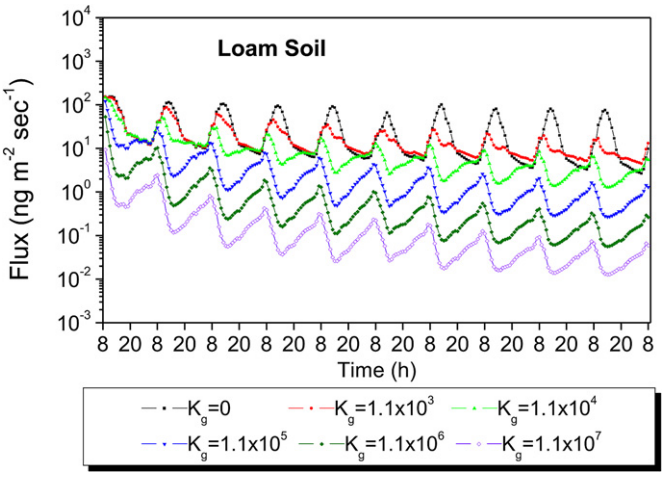

Fig. 6. Influence of the soil air–solid interface partition coefficient value (K_g (m^3 kg^{-1})) on the diurnal pattern of diazinon volatilization rates from loam soil using the BC-D formulation.

a transition point where vapor adsorption strongly affected the simulated flux values (Figs. 6 and 7), this K_g was used below.

The effects of the WR × SSR models on simulated soil temperature and soil-water content, respectively, are summarized in Figs. 3 and 4 for loam soil. The choice of model had no significant effect on calculated soil temperature for either soil (Fig. 3, data not presented for sand). The effect on the soil-water content depended on the soil type and the moisture conditions. For the loam, no significant differences were observed at water contents above the wilting point (0.12 m^3 m^{-3}). For drier soil, a deviation was observed in the simulation, with calculated water contents decreasing in the order: BC-VDG > SG-VDG > BC-D > SG-D (Fig. 4). The deviation between calculated water content values was small as demonstrated by the maximum water content at 0.01 m on day 10, which was 0.088, 0.080, 0.075 and 0.071for BC-VDG, SG-VDG, BC-D and SG-D, respectively. For most WR × SSR combinations, changing the SSR model led to significant changes in water content compared to the WR model. When used with the SG retention function the SSR

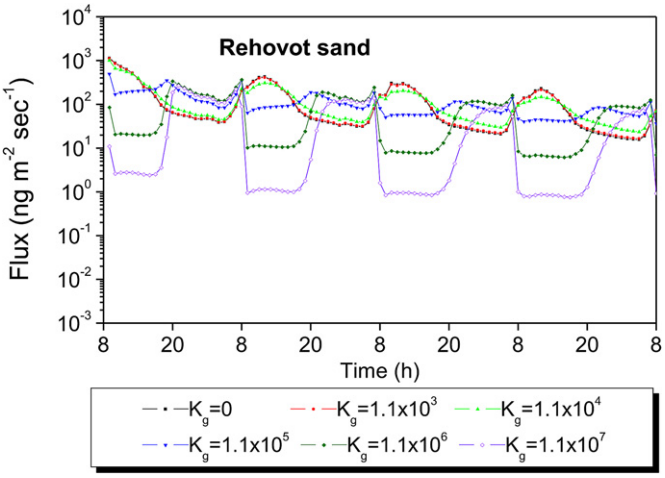

Fig. 7. Influence of the soil air–solid interface partition coefficient value (K_g (m^3 kg^{-1})) on the diurnal pattern of diazinon volatilization rates from Rehovot sand using the BC-D formulation. The curve for $K_g = 0$ (Black) is mostly hidden by the curve for $K_g = 1.1 \times 10^3$ (red). (For interpretation of the references to color in this figure legend, the reader is referred to the web version of this article.)

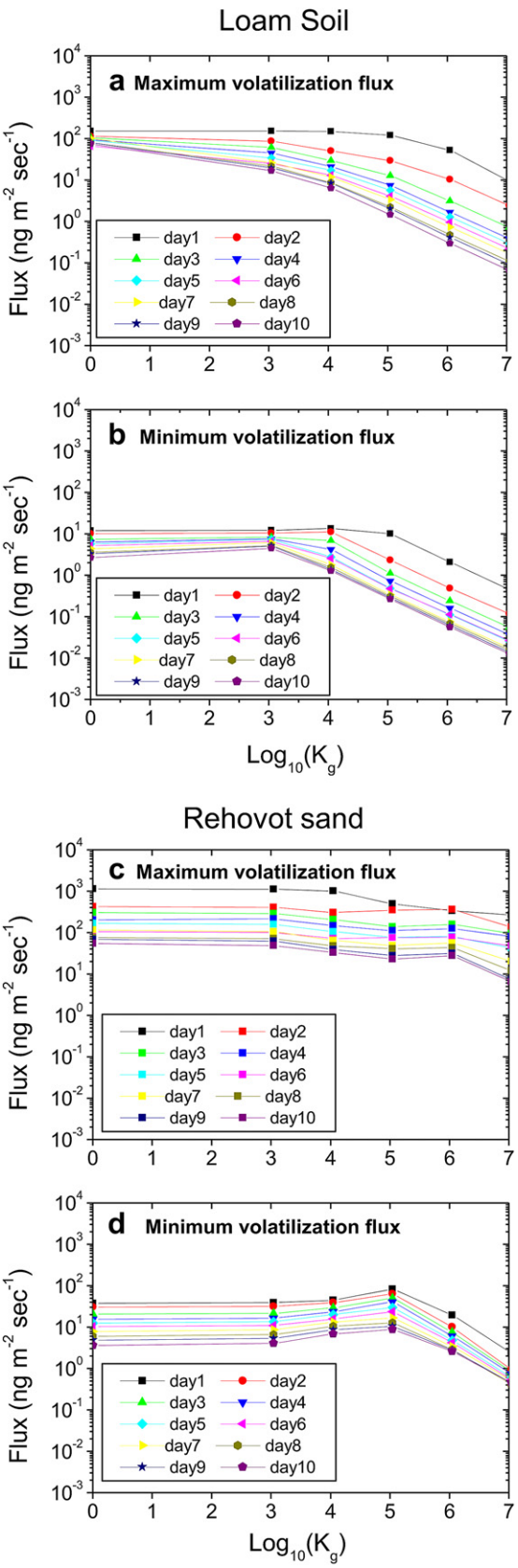

Fig. 8. K_g effect on the maximum volatilization rate peaks for the loam soil (a) and Rehovot sand (c), and the minimum volatilization rate peaks for the loam soil (b) and Rehovot sand (d).

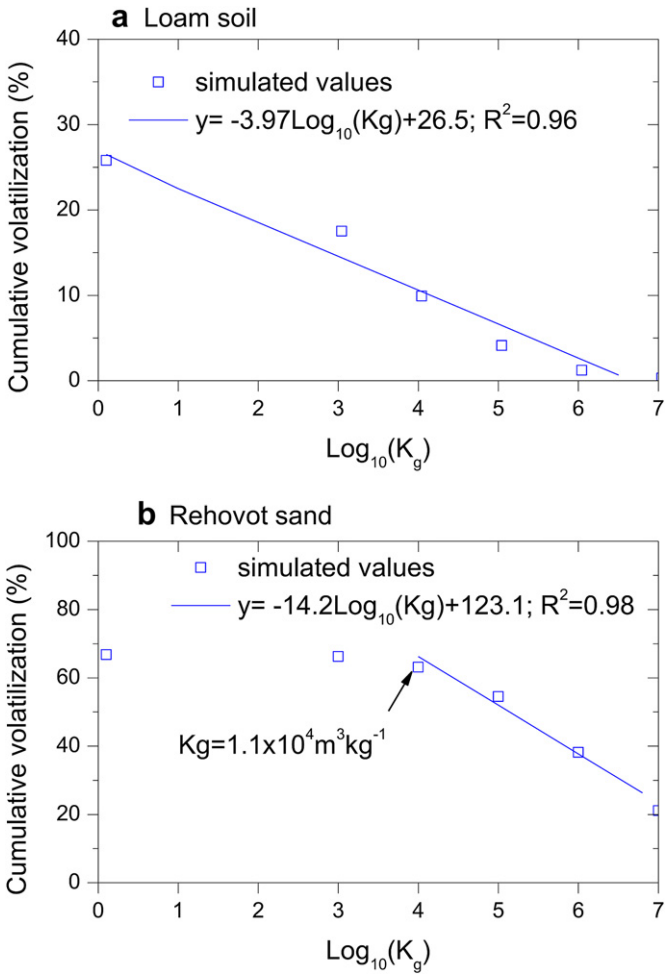

Fig. 9. $Log_{10}(K_g)$ effect on the cumulative flux for (a) loam soil and (b) Rehovot sand.

function had a minor effect. For the sand, significant differences among WR × SSR combinations were observed at all simulated moisture contents. During drying, two distinct outcomes were observed depending on the relationship used for SSR (Fig. 5) with higher calculated water contents for combinations that included the VDG model. For instance, the maximum water content at 0.01 m on day 10 was 0.033, 0.032, 0.027 and 0.027 for BC-VDG, SG-VDG, BC-D and SG-D, respectively. The higher values obtained using the BC WR model are in agreement with the retention curves. For both soils, any given suction value higher than −1.5 MPa (wilting point) will result higher calculated water content values using the BC model (Fig. 1).

The effect of the WR and SSR models on the diurnal variation of diazinon flux is shown in Fig. 10 for loam and Fig. 11 for sand. Similar flux rates were observed for loam under relatively wet conditions. Curve separation was pronounced by the middle of day 3, and followed the behavior of the water content (Fig. 4). The calculated volatilization rates decreased in the following order BC-VDG > SG-VDG > BC-D > SG-D (Fig. 10). The differences in the calculated maximum volatilization rates for day 10 and BC-VDG and SG-VDG, BC-D, SG-D models were 2.38, 1.61, 1.46 and 1.05, ng m^{-2} s^{-1}, respectively. The daily minimum flux rates simulated with the VGD model were relatively wide with two small depressions at 15:00 and 20:00 that eventually become a single minimum at 20:00, as the soil dried.

Greater variation between models was observed in the calculated flux for the Rehovot sand. Two distinct flux patterns that

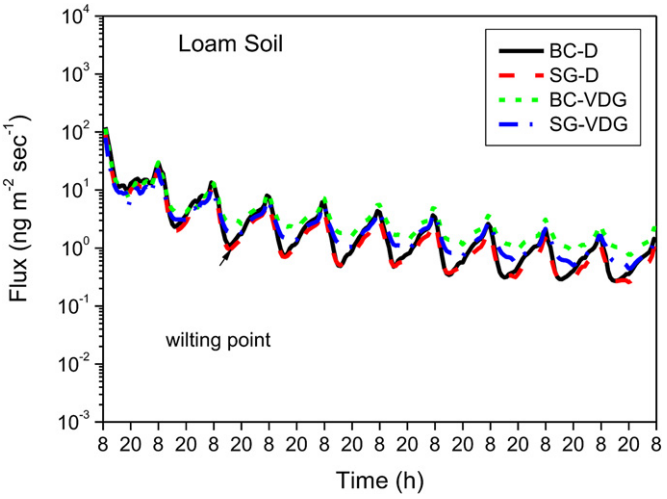

Fig. 10. The effect of the tested models on the simulated diurnal pattern of diazinon volatilization rates from loam soil. $K_g = 1.1 \times 10^5$ (BC = Brooks–Corey water retention function; SG = Silva and Grifoll (2007) full-range water retention model; D = the β wetness surface resistance function of Deardorff (1978); VDG = the surface resistance function proposed by van de Griend and Owe (1994)).

differed in timing and magnitude were observed and depended on the SSR model. When the D model was used, initial flux rates (500 ng m^{-2} s^{-1}) were lower than the VDG model (700 ng m^{-2} s^{-1}), the diurnal peak flux rate occurred around 7:00 and decreasing flux rate was observed during the daytime hours as the soil dried. These results agree with the lower calculated water content values obtained for combinations that included the D model (Fig. 5). Lower flux rates are expected for dryer soil conditions due to increased adsorption. When the VDG model was used, the flux curve followed the diurnal pattern of solar radiation (Fig. 2) during the first three days with high flux rates observed mid-day (12:00). As the soil dried (days 4–6), the diurnal peak flux occurred earlier and a secondary peak was observed at 20:00. Afterward, the soil-water content was about 0.04 m^3 m^{-3} and low fluxes were observed during the daytime hours and high fluxes at night.

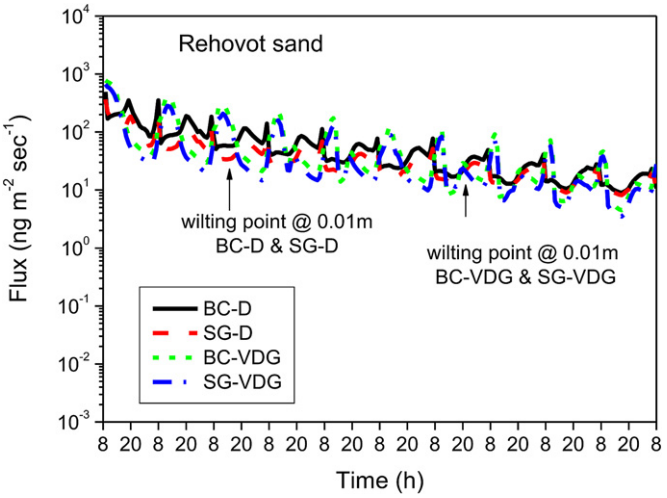

Fig. 11. The effect of the tested models on the simulated diurnal pattern of diazinon volatilization rates from Rehovot sand. $K_g = 1.1 \times 10^5$ (BC = Brooks–Corey water retention function; SG = Silva and Grifoll (2007) full-range water retention model; D = the β wetness surface resistance function of Deardorff (1978); VDG = the surface resistance function proposed by van de Griend and Owe (1994)).

The significant aspect of the effect of the SSR models on soil-water content and pesticide volatilization is that they were formulated to directly track the process of soil surface drying and translate it into boundary resistance that is directly correlated to evaporation and pesticide volatilization rates. The WR models, on the other hand, convert soil suction to water content at the pore scale. They affect the evaporation rate through the value of surface water content, which has lesser impact on water evaporation rate compared to the surface resistance term.

The model and simulations presented herein were tested in a companion paper (Reichman et al., 2013) with an experimental dataset collected in a field study that measured the effect of soil moisture on diazinon volatilization for a Yolo silt loam (Reichman et al., 2011). The results indicate that under very dry conditions, when soil-water content in the top 0.01 m was below the volumetric threshold value, the use of full-range WR function proposed by Silva and Grifoll (2007) resulted in the most accurate prediction of pesticide emission rates. Otherwise, the Brooks–Corey (BC) function was found to be adequate. For simulating pesticide emission under normal conditions, where initial soil moisture is near field capacity or higher, the BC-VDG model should be sufficient. The effect of the SSR function on the prediction accuracy depends on the WR function used and the soil moisture. Under wet conditions, the BC function used in conjunction with the VDG function resulted in more accurate predictions, while in dry conditions the BC-D combination was more accurate. Similar to the current study results, the SSR function had a minor effect when used with the SG retention function, the different models did not affect the soil temperature predictions, and had a minor effect on the predicted soil-water content (like the loam results).

4. Conclusions

A numerical study of the diurnal variation of pesticide emissions as affected by pesticide vapor adsorption to soil particles and soil moisture modeling was conducted using of a comprehensive non-isothermal simulation model. Two water retention (WR) functions, two soil surface resistance (SSR) functions, the properties of diazinon, and a loam or sand soil were considered. Simulations were performed for ten successive days of drying under typical summer conditions of Israel to test the effect of soil water content and the air–solid interface partition coefficient (K_g) on the diurnal diazinon flux rates.

Results show that the temporal variation and the magnitude of diazinon emissions were strongly affected by vapor sorption (K_g), soil-water content, soil properties and SSR model. The displacement of the diurnal peak flux values from mid-day to early morning hours was directly related to K_g and prevailing soil-water content. The effect of K_g was relatively small when the soil-water content at 0.01 m was higher than the wilting point.

Generally, flux rates were of the same order of magnitude for both SSR models. The highest deviation was observed for sand at mid-day under relatively wet conditions, where simulated flux with the VDG method was 5 times larger than the D model. For the simulations conducted herein, the WR functions had a minor effect on water content and volatilization rates. However, for other soil types and conditions WR may be important. The simulated soil temperature was not affected by WR and SSR functions.

This study demonstrates that field scale pesticide emissions may have peak emission rates during the day, or at night, and the timing is related to the soil-water content and vapor-solid sorption. The results also suggest that comprehensive water, heat and solute transport models are needed to accurately simulate pesticide emissions under arbitrary conditions and the use of simpler models may lead to erroneous short-term emission rates.

Disclaimer

The use of trade, firm, or corporation names in this paper is for the information and convenience of the reader. Such use does not constitute an official endorsement or approval by the United States Department of Agriculture or the Agricultural Research Service of any product or service to the exclusion of others that may be suitable.

References

Avissar, R., Mahrer, Y., 1982. Verification study of a numerical greenhouse microclimate model. Trans. ASAE 25, 1711–1720.

Avissar, R., Mahrer, Y., 1988. Mapping frost-sensitivity areas with three-dimensional local-scale numerical model. Part II: comparison with observations. J. Appl. Meteorol. 27, 414–426.

Baker, J.M., Koskinen, W.C., Dowdy, R.H., 1996. Volatilization of EPTC: simulation and measurement. J. Environ. Qual. 25, 169–177. http://dx.doi.org/10.2134/jeq1996.00472425002500010022x.

Bedos, C., Genermont, S., Le Cadre, E., Garcia, L., Barriuso, E., Cellier, P., 2009. Modeling pesticide volatilization after soil application using the mechanistic model volt'air. Atmos. Environ. 43, 3630–3639. http://dx.doi.org/10.1016/j.atmosenv. 2009.03.024.

Bird, R.B., Stewart, W.E., Lightfoot, E.N., 1960. Transport Phenomena. John Wiley and Sons, New York.

Bittelli, M., Ventura, F., Campbell, G.S., Snyder, R.L., Gallegati, F., Pisa, P.R., 2008. Coupling of heat, water vapor, and liquid water fluxes to compute evaporation in bare soils. J. Hydrol. 362, 191–205. http://dx.doi.org/10.1016/j.jhydrol.2008.08.014.

Bradley, R.S., 1936. Polymolecular adsorbed films. J. Chem. Soc. 139, 1467–1474.

Brooks, R.H., Corey, A., 1964. Hydraulic Properties of Porous Media. In: Hydrol. Pap. 3. Colo. State Univ., Fort Collins.

Bro-Rasmussen, F., Nbddegaard, E., Voldum-Clausen, K., 1970. Comparison of the disappearance of eight organophosphorus insecticides from soil in laboratory and in outdoor experiments. Pestic. Sci. 1, 179–182.

Businger, J.A., 1973. Turbulent transfer in the atmospheric surface layer. In: Hugen, D.A. (Eds.), Workshop on Micrometeorology. American Meteorological Society, Boston, MA, pp. 67–100.

Chen, D., Rolston, D.E., 2000. Coupling diazinon volatilization and water evaporation in unsaturated soils: II. Diazinon transport. Soil Sci. 165, 690–698. http://dx.doi.org/10.1097/00010694-200009000-00002.

Chen, D., Rolston, D.E., Yamaguchi, T., 2000. Calculating partition coefficients of organic vapors in unsaturated soil and clays. Soil Sci. 165, 217–225. http://dx.doi.org/10.1097/00010694-200003000-00004.

De Vries, D.A., 1963. Thermal properties of soils. In: van Wijk, W.R. (Ed.), Physics of Plant Environment. North-Holland Publ. Co., Amsterdam, pp. 210–235.

Deardorff, J.W., 1978. Efficient prediction of ground surface temperature and moisture, with inclusion of a layer of vegetation. J. Geophys. Res. 83, 1889–1903.

Fuller, E.N., Schettler, P.D., Giddings, J.C., 1966. A new method for prediction of binary gas-phase diffusion coefficient. Ind. Eng. Chem. 58, 19–27.

Gish, T.J., Prueger, J.H., Kustas, W.P., Daughtry, C.S.T., McKee, L.G., Russ, A., Hatfield, J.L., 2009. Soil moisture and metolachlor volatilization observations over three years. J. Environ. Qual. 38, 1785–1795. http://dx.doi.org/10.2134/jeq2008.0276.

Glotfelty, D.E., Taylor, A.W., Turner, B.C., Zoller, W.H., 1984. Volatilization of surface-applied pesticides from fallow soil. J. Agric. Food Chem. 32, 638–643.

Glotfelty, D.E., Leech, M.M., Jersey, J., Taylor, A.W., 1989. Volatilization and wind erosion of soil surface applied atrazine, simazine, alachlor, and toxaphene. J. Agric. Food Chem. 37, 546–551.

Kim, Y., Woodrow, J.W., Seiber, J.N., 1984. Evaluation of a gas chromatographic method calculating vapor pressures with organophosphorus pesticides. J. Chromatogr. 314, 37–53.

La Mer, V.K., Healy, T.W., 1965. Evaporation of water: its retardation by monolayers. Science 148, 36–41.

Lee, T.J., Pielke, R.A., 1992. Estimating the soils surface specific humidity. J. Appl. Meteorol. 31, 480–484.

Lin, S.Y., Lin, L.W., Chang, H.C., Ku, Y., 1996. Adsorption kinetics of diazinon at the air–water interface. J. Phys. Chem. 100, 16678–16684.

Millington, R.J., Quirk, J.M., 1961. Permeability of porous solids. Trans. Faraday Soc. 57, 1200–1207.

Moldrup, P., Olesen, T., Schjønning, P., Yamaguchi, T., Rolston, D.E., 2000. Predicting the gas diffusion coefficient in undisturbed soil from soil water characteristics. Soil Sci. Soc. Am. J. 64 (1), 94–100. http://dx.doi.org/10.2136/sssaj2000.64194x.

Mualem, Y., 1976. A new model for predicting the hydraulic conductivity of unsaturated porous media. Water Resour. Res. 12, 513–522.

Orchiston, H.D., 1952. Adsorption of water vapor: I. Soils at 25 °C. Soil Sci. 76, 453–465.

Pattey, E., Cessna, A.J., Desjardins, R.L., Kerr, L.A., Rochette, P., St-Amour, G., Zhu, T., Headrick, K., 1995. Herbicides volatilization measured by the relaxed eddy accumulation technique using two trapping media. Agric. For. Meteorol. 76, 201–220.

Philip, J.R., de Vries, D.A., 1957. Moisture movement in porous materials under temperature gradients. Eos Trans. AGU 38, 222–231.

Prueger, J.H., Gish, T.J., McConnell, L.L., Mckee, L.G., Hatfield, J.L., Kustas, W.P., 2005. Solar radiation, relative humidity, and soil water effects on metolachlor volatilization. Environ. Sci. Technol. 39, 5219–5226. http://dx.doi.org/10.1021/es048341q.

Rawls, W.J., Brakensiek, D.L., Sexton, K.E., 1982. Estimation of soil water properties. Trans. ASAE 25, 1316–1320.

Reichman, R., Wallach, R., Mahrer, Y., 2000. A combined soil-atmosphere model for evaluating the fate of surface-applied volatile organic chemicals. 1. Model development and verification. Environ. Sci. Technol. 34 (7), 1313–1320. http://dx.doi.org/10.1021/es990356e.

Reichman, R., Rolston, D.E., Yates, S.R., Skaggs, T.H., 2011. Diurnal variation of diazinon volatilization: soil moisture effects. Environ. Sci. Technol.. http://dx.doi.org/10.1021/es102921r

Reichman, R., Yates, S.R., Skaggs, T.H., Rolston, D.E., 2013. Effects of soil moisture on the diurnal pattern of pesticide emission: comparison of simulations with field measurements. Atmos. Environ. 66, 52–62.

Ruiz, J., Bilbao, R., Murillo, M.B., 1998. Adsorption of different VOC onto soil minerals from gas phase: influence of mineral, type of VOC, and air humidity. Environ. Sci. Technol. 32, 1079–1084. http://dx.doi.org/10.1021/es9704996.

Schneider, M., Goss, K.-U., 2011. Temperature dependence of the water retention curve for dry soils. Water Resour. Res. 47, W03506. http://dx.doi.org/10.1029/2010WR009687.

Scholtz, M.T., Voldner, E., McMillan, A.C., Van Heyst, B.J., 2002a. A pesticide emission model (PEM) part I: model development. Atmos. Environ. 36, 5005–5013. http://dx.doi.org/10.1016/S1352-2310(02)00570-8.

Scholtz, M.T., Voldner, E., Van Heyst, B.J., McMillan, A.C., Pattey, E., 2002b. A pesticide emission model (PEM) part II: model evaluation. Atmos. Environ. 36, 5015–5024. http://dx.doi.org/10.1016/S1352-2310(02)00571-X.

Silva, O., Grifoll, J., 2007. A soil-water retention function that includes the hyper-dry region through the BET adsorption isotherm. Water Resour. Res. 43, W11420. http://dx.doi.org/10.1029/2006WR005325.

Spencer, W.F., Cliath, M.M., 1970. Desorption of lindane from soil as related to vapor density. Soil Sci. Soc. Am. Proc. 34, 574–578.

Spencer, W.F., Cliath, M.M., 1973. Pesticide volatilization as related to water loss from soil. J. Environ. Qual. 2, 284–289. http://dx.doi.org/10.2134/jeq1973.00472425000200020026x.

Spencer, W.F., Cliath, M.M., Farmer, W.J., 1969. Vapor density of soil-applied dieldrin as related to soil-water content, temperature, and dieldrin concentration. Soil Sci. Soc. Am. Proc. 33, 509–511. http://dx.doi.org/10.2136/sssaj1969.03615995003300040010x.

Spencer, W.F., Farmer, W.J., Jury, W.A., 1982. Review: behavior of organic chemicals at soil, air, water interfaces as related to predicting the transport and volatilization of organic pollutants. Environ. Toxicol. Chem. 1, 17–26.

Taylor, A.W., Spencer, W.F., 1990. Volatilization and vapor transport processes. In: Pesticides in the Soil Environment: Processes, Impacts and Modeling. Soil Science Society of America Book Series, No. 2. SSSA, Madison, WI, pp. 213–269 (Chapter 7).

van de Griend, A., Owe, M., 1994. Bare soil surface resistance to evaporation by vapor diffusion under semiarid conditions. Water Resour. Res. 30 (2), 181–188.

Wang, D., Yates, S.R., Gan, J., 1997. Temperature effect on methyl bromide volatilization in soil fumigation. J. Environ. Qual. 26, 1072–1079. http://dx.doi.org/10.2134/jeq1997.00472425002600040019x.

Wang, D., Yates, S.R., Jury, W.A., 1998. Temperature effect on methyl bromide volatilization: permeability of plastic cover films. J. Environ. Qual. 27, 821–827. http://dx.doi.org/10.2134/jeq1998.00472425002700040015x.

Yates, S.R., 2006. Simulating herbicide volatilization from bare soil affected by atmospheric conditions and limited solubility in water. Environ. Sci. Technol. 40, 6963–6968. http://dx.doi.org/10.1021/es061303h.